Spatiotemporal chaos in a model of Rayleigh-Bénard convection

Haowen Xi
Exxon Research and Engineering Company, Annandale, New Jersey 08801

J. D. Gunton
Department of Physics, Lehigh University, Bethlehem, Pennsylvania 18015
(Received 6 December 1994; revised manuscript received 4 May 1995)

We present a numerical investigation of mean-flow induced spiral turbulence in a generalized Swift-Hohenberg model in two dimensions. We show the existence of a spatiotemporal chaotic state comprised of a large number of rotating spirals in a large aspect ratio system. This state is not predicted by classical theory. We calculate the spatial correlation functions for the order parameter, vorticity, and mean-flow field in order to characterize more quantitatively the spiral chaos state. Our simulations show that there is a power-law behavior in the temporal dynamics of spiral defect chaos. Our study suggests that this spiral defect state occurs for low Prandtl numbers and large aspect ratios. We use as global variables the spectra entropy and the magnitude of the vorticity to characterize the transition from the global parallel roll state to the localized spiral state. Unfortunately we cannot determine whether this transition is gradual or sharp.

PACS number(s): 47.20.−k, 47.27.−i, 47.32.−y

I. INTRODUCTION

The spatiotemporal chaotic behavior of spatially extended, dissipative systems has drawn considerable interest in recent years [1]. The transition to spatiotemporal chaos has been observed in various physical systems such as Taylor-Couette vortex flow [2], Faraday surface waves [3], traveling waves in binary mixtures convection [4], optical instabilities [5], flames [6], chemical reactions [7], and Rayleigh-Bénard convection [8]. Spatiotemporal chaos (sometimes called weak turbulence) results from a breakdown of global spatial coherence. However, a macroscopic *coherence length*—a length scale below which the pattern appears coherent—may still be observed. Recently, a transition from a global parallel roll state to a chaotic spiral defect pattern (which we will refer to loosely as spiral chaos below) has been observed in Rayleigh-Bénard convection in both a Boussinesq and non-Boussinesq fluid (CO_2 gas) [9,10], for a large aspect ratio system, at moderate Rayleigh numbers and low Prandtl number. The spiral chaos state has also been observed in the convective fluid of SF_6 [11]. In previous experiments on convection in CO_2 gas [12], the spontaneous formation of a *global* rotating spiral pattern state was observed at a lower Rayleigh number. The chaotic state observed more recently in the experiment [9] is comprised of a large number of rotating spirals. Spirals nucleate, interact, and annihilate, yielding a macroscopically disordered pattern. There have been several previous numerical investigations of global spiral and spiral chaos states by using a generalized Swift-Hohenberg equation [13–16]. We found that chaotic spiral patterns are spontaneously formed during the transition from the conduction state to the convective roll state, in agreement with the experimental observations. An interesting issue raised by the experiments and simulations is to identify the mechanism responsible for spiral chaos. The stationary parallel roll state and the secondary instabilities have been obtained by Busse [17]. However, his classical theory [17] does not predict spiral chaos states. We are not able to identify the origin of spiral chaos in this paper. Another interesting issue raised by the experiments and simulations is the nature of the transition from the globally ordered parallel roll state to the globally disordered but *locally* ordered spiral chaos state, which we study in this paper. Pomeau [18] has proposed that the transition to spatiotemporal chaos in an extended dissipative system generally occurs in one of two ways. The first scenario involves a "supercritical transition," characterized by the development of velocity and temperature fluctuations at approximately the same rate throughout the ordered (laminar) system. The second scenario is a "subcritical transition," where the disorder (turbulence) occurs in localized patches in time and space, and the system exhibits coexistence regimes of order ("laminar") and disorder ("turbulence"). Although our results are qualitatively consistent with Pomeau's "supercritical transition," we are not able to confirm this in detail, in that we cannot distinguish between a gradual and a sharp transition.

In this paper we extend the work reported in Ref. [14] to examine several additional features. These include a study of the spiral chaos state as a function of the Rayleigh number and for two values of the Prandtl number. This includes a study of the transition from the parallel roll to the spiral state. We study the vorticity energy and spectra entropy near the onset of the spiral chaos state as a way to characterize quantitatively the transition. As we noted above we cannot confirm Pomeau's scenario of a supercritical transition, although our results are not inconsistent with this picture. Our results for the large scale mean-flow field, vertical vorticity, and the temporal dynamics of the spiral state have

not yet been studied experimentally. Since sidewalls are known to play an important role in pattern formation in Rayleigh-Bénard convection, we also study the effects of sidewall forcing in this paper. Our work strongly suggests that the spiral chaos state is indeed an intrinsic property of the system. That is, this state does not arise from confinement effects due to the sidewall. We also note that our work involves a larger aspect ratio than in our previous study and is comparable to the experiment.

Recently, Decker, Pesch, and Weber [19] have also studied spiral-defect chaos in Rayleigh-Benard convection, starting from a more complete description of this problem than that which is given by the generalized Swift-Hohenberg model that we study [14]. Their starting point is the Boussinesq approximation for the full hydrodynamic equations with realistic rigid-rigid boundary conditions. They project these equations onto vertical modes and eliminate the dependence on the vertical coordinate z (this dependence is thought to be irrelevant) leave a dependence on time t and the two remaining horizontal coordinates x, y only. They then make an approximation and assume that only the first few modes are relevant for the dynamics. Their model equations essentially consist of a set of three partial differential equations coupled by their nonlinear terms. The first equation governs the vertical velocity of the convective flow, the second equation accounts for the large scale mean flow alluded to above, and the third equation describes the temperature field with a nonlinear coupling to the flow velocity. To compare their model with ours, it is important to realize that the Swift-Hohenberg model that we study is a real space approximation of the Fourier transform form. An accurate solution requires an exact inversion in Fourier space, but leads to a complicated convolution. The real space approximation to the exact inversion that we use is the main difference between the model of Decker *et al.* and our Swift-Hohenberg model, although both methods apply the projection method and reduce the original three-dimensional hydrodynamic equations to a two-dimensional problem. Decker *et al.* treat the nonlinear terms exactly for the system, whereas we make a real space approximation. It is clear that their treatment has several advantages over our previous and current work, in that the model reproduces the Busse balloon, whereas the corresponding stability limits for our model differ from the Busse balloon. Also, our model has an unphysical short-wavelength cross roll instability, which means that our results for large q are inaccurate. On the other hand, our model has the advantage of incorporating large scale numerical simulation, so that we can examine the dependence of spiral chaos on the two control parameters for the system (the reduced Rayleigh number and Prandtl number, respectively). Also, we can simulate the experimentally interesting case of large aspect ratio. Finally, we note that it is straightforward to calculate the analog of the Busse balloon for our model. We have done so and found the results are essentially the same as found by Greenside and Cross [22] for a quite similar model. We refer the interested reader to their paper for the details of the stability diagram.

The rest of the paper is organized as follows. In Sec. II, we give a brief description of the theoretical model used to describe the spiral chaos pattern formation in Rayleigh-Bénard systems. In Sec. III we present various numerical results and show spatiotemporal spiral chaos pattern formation. We also show that the power spectrum of the convective current has a power-law behavior, f^{-2}, at large frequency f. In Sec. IV, we study the transition from a global parallel roll state to a spatiotemporal spiral chaos state, and address the question of the nature of this phase transition. In Sec. V, we present a brief conclusion.

II. A TWO-DIMENSIONAL MODEL FOR RAYLEIGH-BÉNARD CONVECTION

We model Rayleigh-Bénard convection by a two-dimensional generalized Swift-Hohenberg model [20,21], defined by Eqs. (1)–(4) below, which we solve by numerical integration. The Swift-Hohenberg equation and various generalizations of it have proven to be quite successful in explaining many of the features of convective flow in fluids, particularly near onset [22,23,15]. Our model is defined in dimensionless units by

$$\frac{\partial\psi(\vec{r},t)}{\partial t} + g_m\vec{U}\cdot\vec{\nabla}\psi = \left[\epsilon' - \left(\nabla^2+1\right)^2\right]\psi - g_2\psi^2 - \psi^3, \tag{1}$$

$$\left[\frac{\partial}{\partial t} - \mathrm{Pr}(\nabla^2 - c^2)\right]\nabla^2\zeta = \left[\vec{\nabla}(\nabla^2\psi)\times\vec{\nabla}\psi\right]\cdot\hat{\vec{e}}_z, \tag{2}$$

where $\vec{U}$ is the mean-flow velocity,

$$\vec{U} = (\partial_y\zeta)\hat{\vec{e}}_x - (\partial_x\zeta)\hat{\vec{e}}_y. \tag{3}$$

The boundary conditions are,

$$\psi|_B = \hat{\vec{n}}\cdot\vec{\nabla}\psi|_B = \zeta|_B = \hat{\vec{n}}\cdot\vec{\nabla}\zeta|_B = 0, \tag{4}$$

where $\vec{n}$ is the unit normal to the boundary of the domain of integration, B. Equation (1) with $g_2 = g_m = 0$ reduces to the Swift-Hohenberg (SH) equation. The scalar order parameter $\psi(\vec{r},t)$ is related to the fluid temperature in the midplane of the convective cell, g_2 is the "non-Boussinesq parameter," and $\zeta(\vec{r},t)$ is the vertical vorticity potential where the vertical component of the vorticity ω_z is given by $\omega_z = (\vec{\nabla}\times\vec{V})_z = -\nabla^2\zeta$. Thus Eq. (2) is an equation of motion for ω_z. Mean flow arises when ω_z is driven by roll curvature and amplitude modulations. Coupling to mean flow has been shown to play a key role, for example, in the onset of weak turbulence in Boussinesq fluids [21,24,25]. The quantity ϵ' is the scaled control parameter, $\epsilon' = (\frac{4}{k_c^2\xi_0^2})\epsilon_{\mathrm{expt}}$, where $\epsilon_{\mathrm{expt}} = (\frac{R}{R_c} - 1)$ is the reduced Rayleigh number. Here R is the Rayleigh number, R_c is the critical Rayleigh number for an infinite system, k_c is the critical wave number, ξ_0 is the characteristic length scale, Pr is the Prandtl number, and c^2 is an unknown constant. We note [26] that the dimensionless time t in Eqs. (1) and (2) is related to the experimental

time τ by $t = (\frac{k_c^2 \xi_0^2}{4\tau_0})\tau/(d^2/\kappa)$, where d is the cell thickness, $k_c = 3.117$, ξ_0^2=0.148, $\tau_0 = 0.076\,93$ (for Pr=1.0) for the rigid-rigid boundary condition, and κ is the thermal diffusity.

The values of g_2 and Pr that enter the equation have been chosen in the range appropriate for earlier experiments of Bodenschatz *et al.* on CO_2 [12]. In order to approximate g_2 in terms of experimentally measurable quantities, we have derived a three mode amplitude equation from the generalized Swift-Hohenberg equation. From the experiments described in [12], we have estimated $g_2 \approx 0.35$. We have chosen $g_m \approx 50$ which is about four times the estimated experimental value. (If we use the experimental value of g_m, we see spiral chaos at a large value $\epsilon' > 1$, but this value of ϵ' is beyond the expected range of validity of the Swift-Hohenberg equation.) The value of ϵ' used in the numerical simulation is 0.7, which is related to the experimental value ϵ_{expt} in Ref. [12] by $\epsilon_{\text{expt}} = 0.3594\epsilon'$=0.2516. We have chosen $c^2 = 2$ to simulate approximately the experimental rigid-

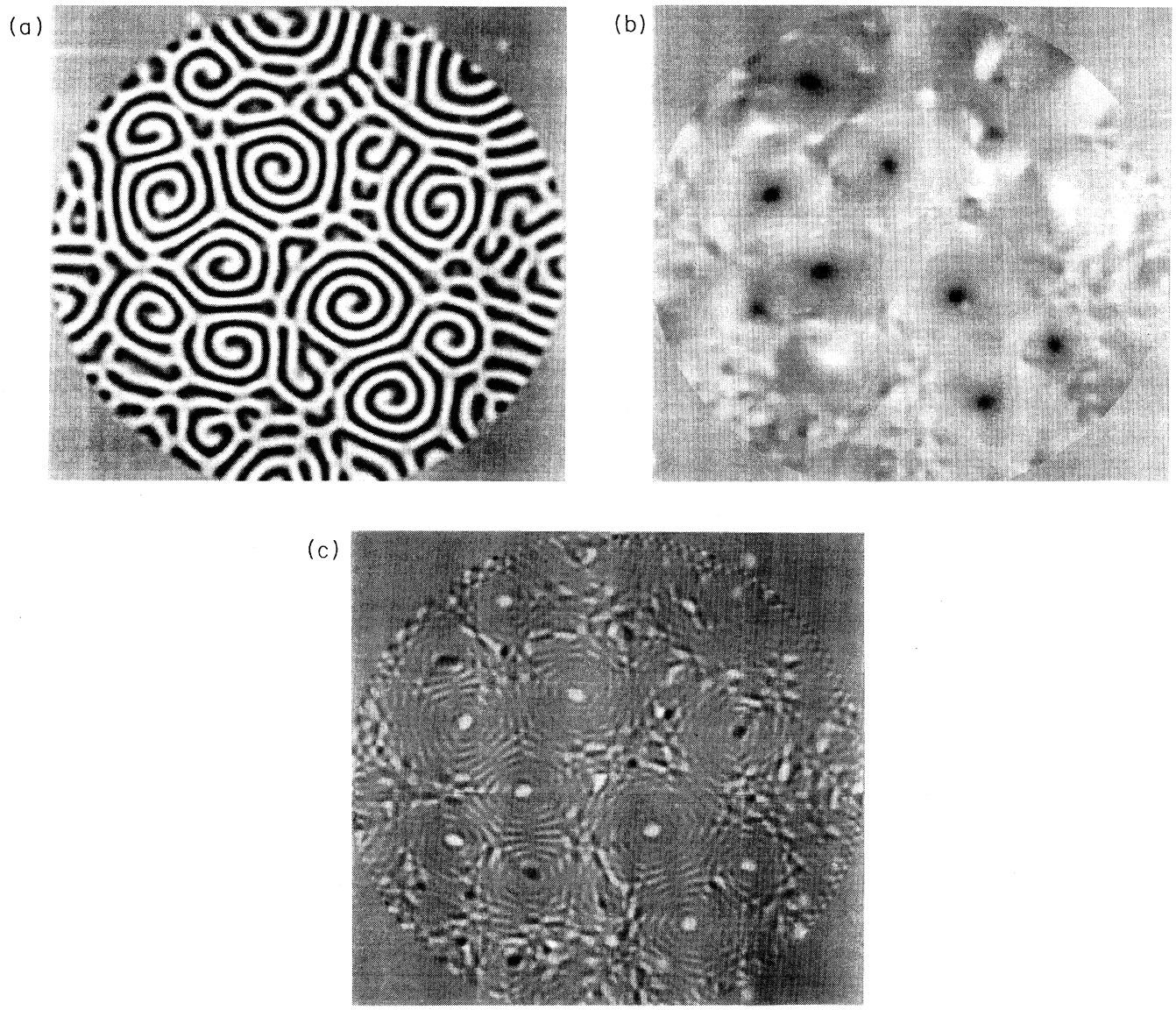

FIG. 1. (a) A typical configuration of the spiral chaos state. Dark regions correspond to hot rising fluid and white regions to cold descending fluid. The field $\psi(x, y, t)$ is shown here. Dark regions correspond to $\psi > 0$ and light regions to $\psi < 0$. (b) A snapshot of the mean-flow field $\zeta(x, y, t)$ that corresponds to the configuration shown in (a). White and dark regions correspond to clockwise and counterclockwise rotation of the spiral, respectively. (c) A snapshot of the vertical vorticity field $\omega_z(x, y, t)$ that corresponds to the configuration shown in (a). White and dark regions correspond to counterclockwise and clockwise rotation of the spiral, respectively. The configuration shown is $t = 900$.

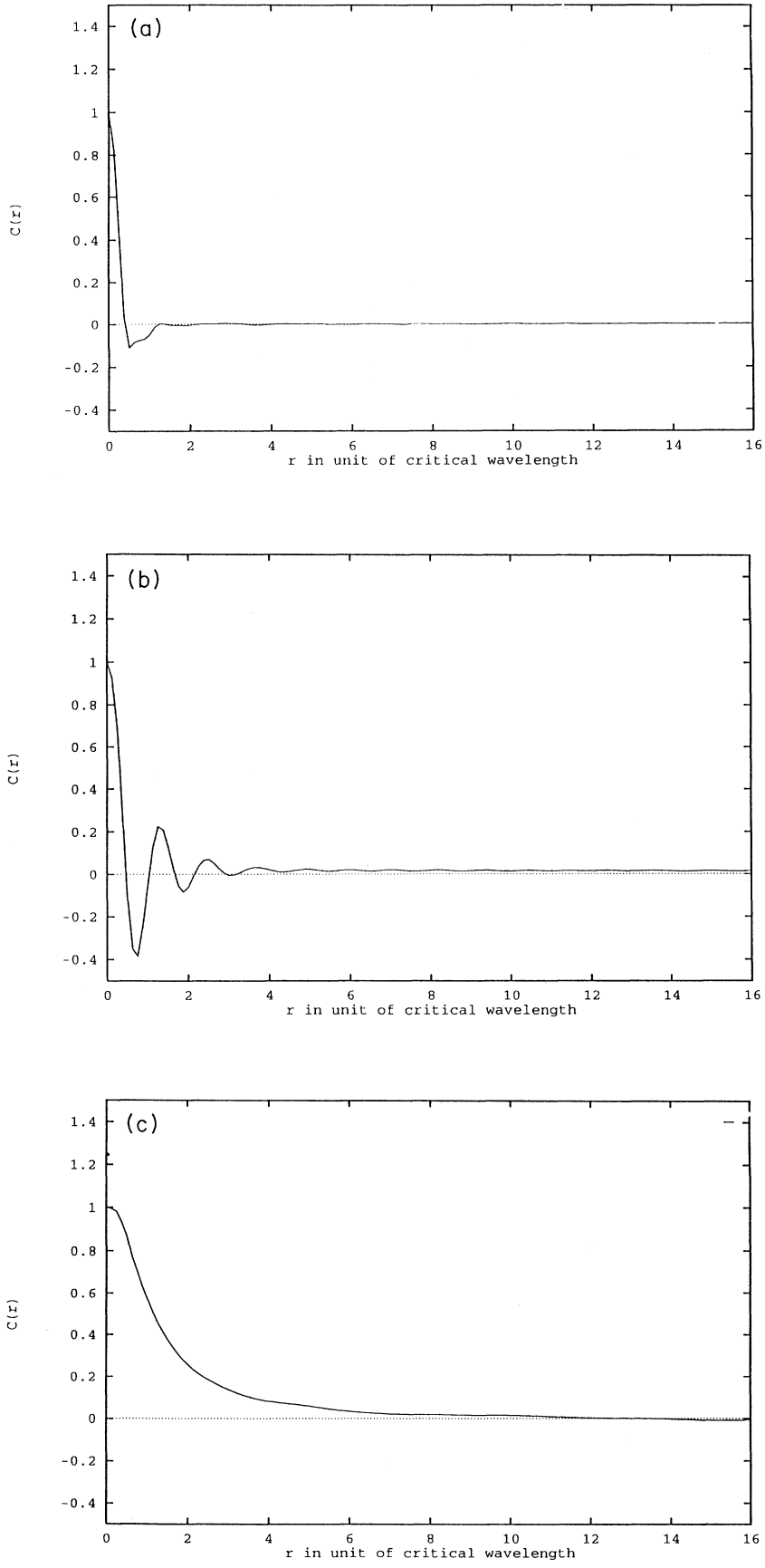

FIG. 2. (a)–(c) Circularly averaged correlation function $\langle C(r) \rangle$ for (a) the vertical vorticity $\langle C_{\omega_z}(r) \rangle$, (b) the velocity field $\langle C_{\psi}(r) \rangle$, and (c) the mean-flow field $\langle C_{\zeta}(r) \rangle$. Here $\langle\ \rangle$ denotes a time average and r is in units of the critical wavelength $\lambda_c = 2\pi/k_c$.

rigid boundary condition. (Note that $c^2 = 0$ corresponds to a free-free boundary condition.)

III. NUMERICAL RESULTS

In this section, we present various numerical studies based on Eqs. (1)–(4) in a large aspect ratio cell. We begin with the study of the spiral chaos pattern formation from the conduction state. We characterize the spiral chaos state by calculating correlation functions of the order parameter $\psi(\vec{r},t)$, the mean-flow field $\zeta(\vec{r},t)$, and vertical vortex field $\omega_z(\vec{r},t)$, respectively. Next, we study the mechanism of formation of the spiral chaos state. We investigate the roles of the non-Boussinesq effect, Prandtl number, aspect ratio of the cell, and sidewall forcing on the formation of the spiral state. We also study the transition from the parallel roll state to the spiral state. We use the spectra entropy and vortex energy to characterize the transition.

We consider as initial condition $[\psi(\vec{r}) = 0]$ a Gaussian random variable with zero mean and variance 10^{-4}. We numerically solve Eqs. (1)–(4) in a circular cell of radius $r = 32\pi$, which corresponds to an aspect ratio $\Gamma = r/\pi = 32$. A grid with N^2 nodes has been used with spacing $\Delta x = \Delta y = 64\pi/N$, and $N = 512$. We approximate the circular boundary conditions on ψ and ζ by taking $\psi(\vec{r},t) = \zeta(\vec{r},t) = 0$ for $||\vec{r}|| \geq D/2$, where $\vec{r}$ is the location of a node with respect to the center of the domain, and D is the diameter of the circular domain.

Our main result is that the GSH model exhibits a spatiotemporal spiral chaos state which spontaneously forms as one changes ϵ' during the transition from the conduction state. This spiral chaos state is remarkably similar

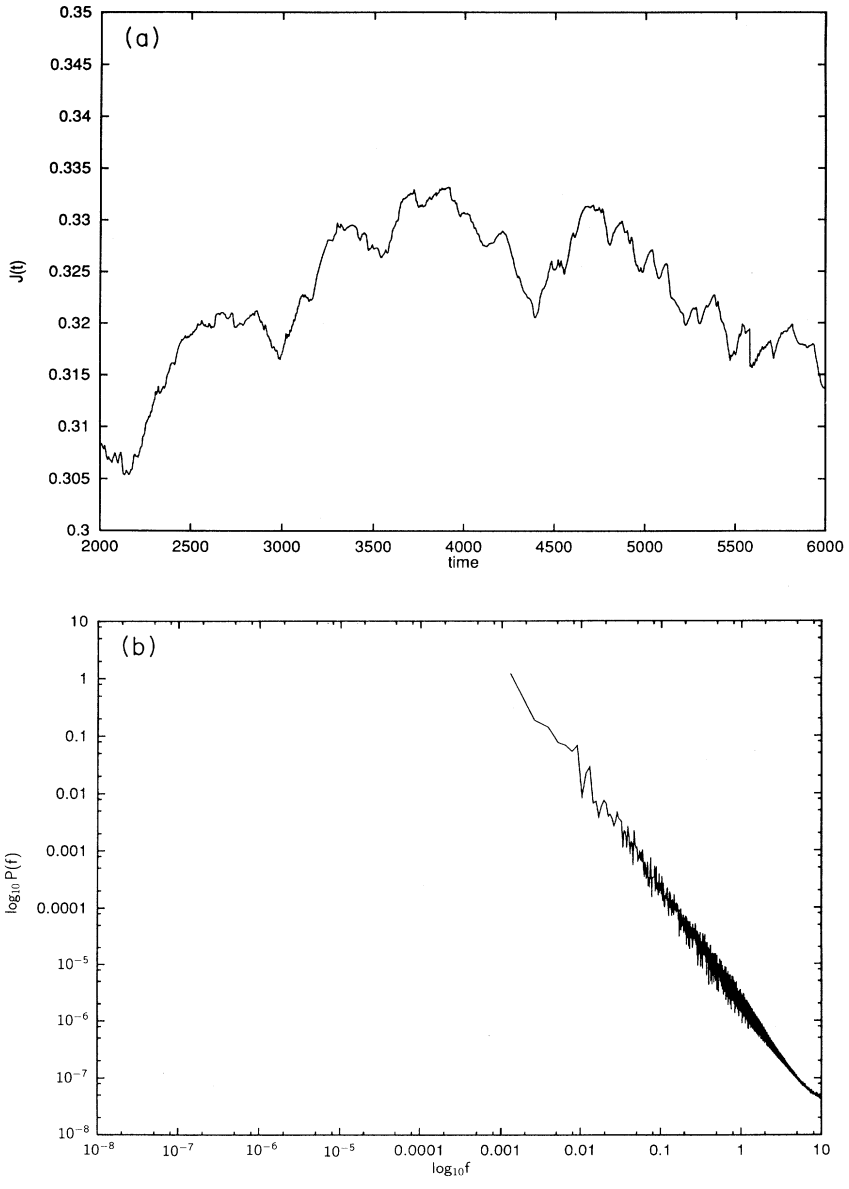

FIG. 3. (a) Time evolution of convective current $J(t)$ for spiral-defects chaos state with aspect ratio $\Gamma = 32$. The values of the parameters used are ϵ'=0.7, $g_2 = 0.35$, $g_m = 50$, Pr=1, and $c^2 = 2$. (b) Power spectrum of the convective current.

in visual appearance to that observed experimentally [9]; there the system was also quenched from the conduction state. Figure 1(a) shows a typical configuration of the spiral chaos state. Dark regions correspond to hot rising fluid and white regions to cold descending fluid. It is now known that the mean-flow field plays a major role in the dynamics of pattern formation in these convective systems. Figures 1(b) and 1(c) show the mean-flow field $\zeta(x,y,t)$ and the vertical vorticity field $\omega_z(x,y,t)$ that correspond to the configuration shown in Fig. 1. White and dark regions in the mean-flow field correspond to clockwise and counterclockwise rotations of the spiral, respectively, and vice versa for the vertical vorticity field. In contrast to the spiral chaos patterns which have spatial order of k_c^{-1}, the vertical vorticity fields are highly localized in space. This suggests that the dynamics of these vorticity fields can be described in term of the dynamics of "particlelike" motion, although we have not attempted to do this.

One of the important ways to characterize spiral chaos is through the correlation function which describes the localized coherent spiral structure. The vorticity-vorticity correlation function $\langle C_{\omega_z}(\vec{r})\rangle$ is shown in Fig. 2(a), where $\langle\,\rangle$ denotes a time average. Its behavior reveals a very compact core structure for the spiral as shown in Fig. 2(a). We also have calculated the corresponding spatial correlation functions $\langle C_\psi(\vec{r})\rangle$ and $\langle C_\zeta(\vec{r})\rangle$. These are shown in Figs. 2(b) and 2(c), respectively. We see from Fig. 2(a) that the circularly averaged $\langle C_\psi(r)\rangle$ has an oscillatory behavior with a corresponding decay of the envelope function that can be fit by an exponential function. If one uses the exponential function to define a correlation length, one finds $\xi = 1.2\lambda_c$ at $\epsilon' = 0.7$, where λ_c is the critical wavelength near onset.

To analyze the temporal dynamics of the spiral-defect chaos state, we use the dimensionless convective heat current $J(t)$ defined as

$$J(t) = \frac{1}{S}\int d^2\vec{r}\psi(\vec{r},t)^2 \ , \tag{5}$$

where S is the dimensionless area of the cell. Figure 3(a) shows a representative time series of $J(t)$ for the spiral-defect chaos pattern. We note that the temporal dynamics has a stochastic behavior and fluctuates around a mean value of $\langle J\rangle$=0.32. The power spectrum of $J(t)$ in Fig. 3(b) clearly shows a power-law $f^{-\alpha}$ behavior, with $\alpha \approx 2$. This result would seem to be of experimental and theoretical interest. Our results here differ from an earlier numerical study of defect dynamics in smaller cells [25], in which a power-law behavior at higher frequencies is observed, with an exponent $\alpha \approx 6$. However, the authors [25] do not study spiral chaos; therefore this difference in exponent values does not seem surprising. It would be of interest to study experimentally this $1/f^2$ noise phenomena in spiral-defect chaos.

The classical work of Busse provides considerable information about the dynamical behavior of the system. In addition to predicting that inside the so-called Busse balloon [17] parallel rolls are stable, his theory also predicts a variety of secondary instabilities. However, his theory does not predict the spiral chaos state that we have studied. As we noted in the Introduction, however, one might ask whether this spiral state is induced by the bending of rolls due to the sidewall. To investigate this equation, we have studied the spiral chaos pattern formation in the presence of the sidewall forcing. The main motivation for such a study is the fact that sidewall forcing will induce a concentric roll state for a cylindrical cell (target pattern)

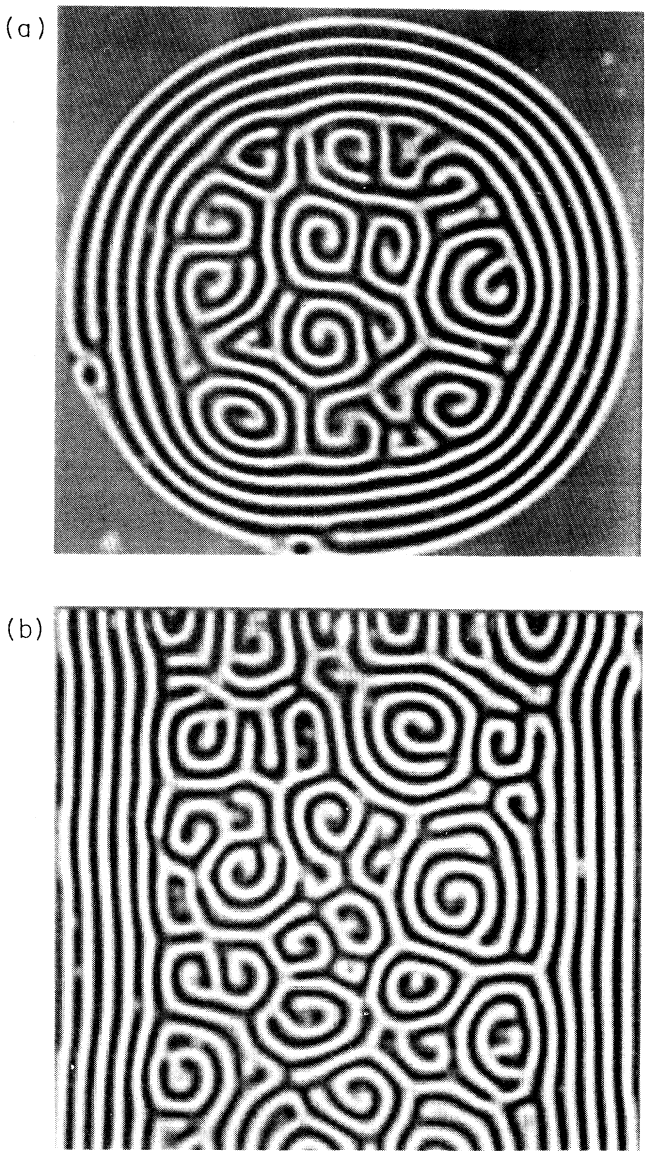

FIG. 4. Spiral chaos pattern formation in the presence of the sidewall forcing in (a) a cylindrical container and (b) a square container. The configuration shown has evolved from random initial conditions with aspect ratio $\Gamma = 32$. The values of the parameters used are $g_2 = 0$, $g_m = 50$, Pr=1, and $c^2 = 2$. The parameter ϵ' is quenched from 0 to 0.7, and a localized force field $f = 0.1$ near the wall was used in the simulation.

or a square roll for a square container in competition with the spiral chaos state [15]. If spiral chaos indeed solely arises from an intrinsic effect, i.e., not induced by confinement effects, then we should observe the spiral chaos state in the presence of the sidewall forcing. This is indeed the case, as shown in Figs. 4(a) and 4(b), in which the spiral chaos pattern is observed both in the circular and square cells with the sidewall forcing.

The Rayleigh-Bénard problem has four independent control parameters, namely the Rayleigh number ϵ_{expt}, the Prandtl number Pr, the aspect ratio Γ, and the nature of the convective fluid, i.e., Boussinesq or non-Boussinesq fluid. To understand other aspects of the formation of the spiral chaos state, we have studied the role of each control parameter on the formation of the spiral chaos state, and conclude that only a large mean-flow field, i.e., small Prandtl numbers, and large aspect ratios (large enough compared with the average size of a coherent spiral structure), are relevant for the existence of the spiral chaos state.

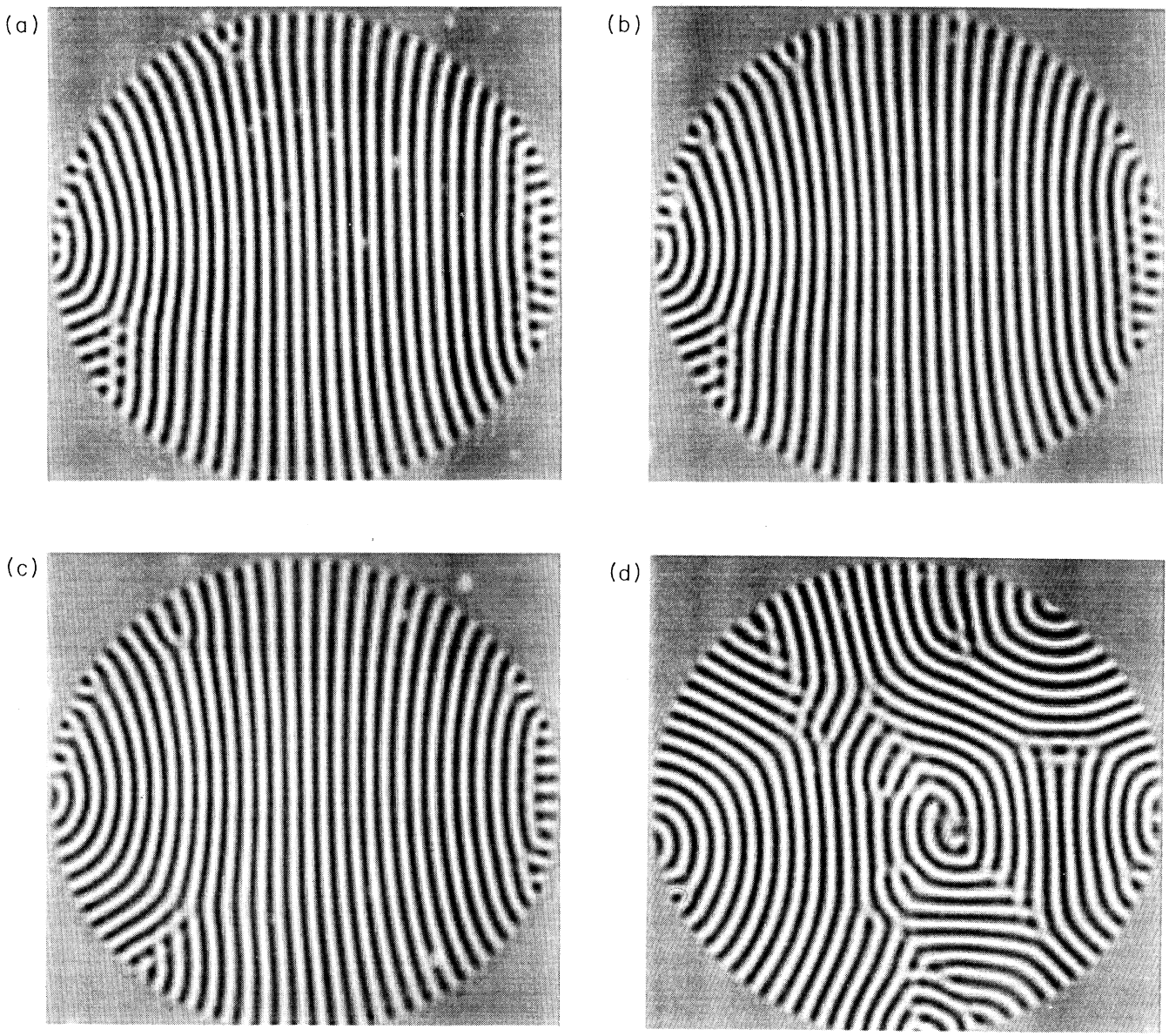

FIG. 5. (a)–(j) This sequence of configurations shows the typical convective pattern as a function of the control parameter ϵ'. One may distinguish between two different regimes: one is dominated by the global parallel roll state, the other is dominated by the spiral chaos state. The transition from global parallel roll to spiral chaos state occurs when $\epsilon'_c \approx 0.25$. The control parameters are (a) ϵ'=0.2, (b) ϵ'=0.22, (c) ϵ'= 0.25, (d) ϵ'= 0.27, (e) ϵ'= 0.3, (f) ϵ'= 0.35, (g) ϵ'= 0.4, (h) ϵ'= 0.5, (i) ϵ'= 0.6, and (j) ϵ'= 0.7. The values of the other parameters used are $g_2 = 0.35$, $g_m = 50$, $c^2 = 2$, and Pr=1.

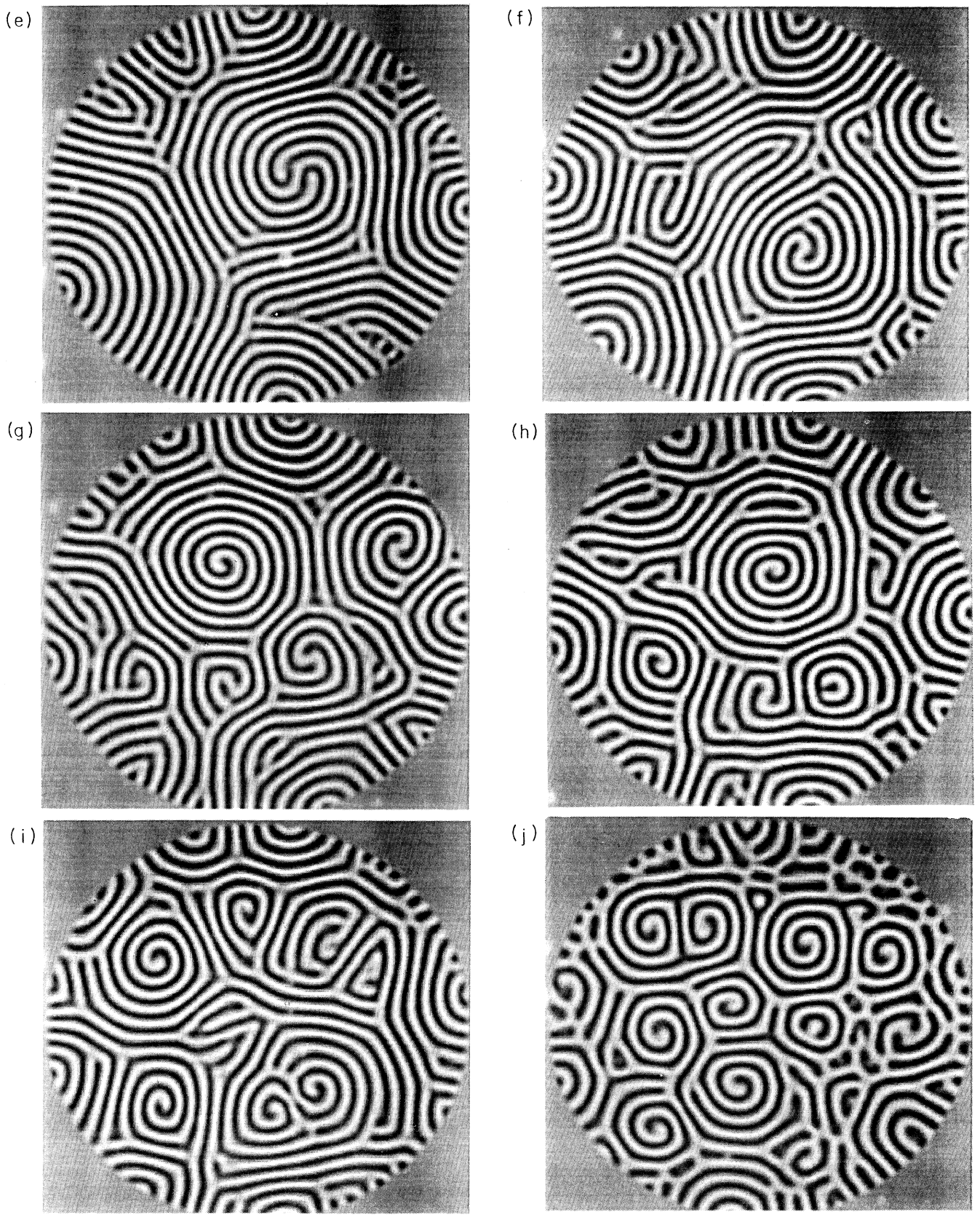

FIG. 5. (*Continued*).

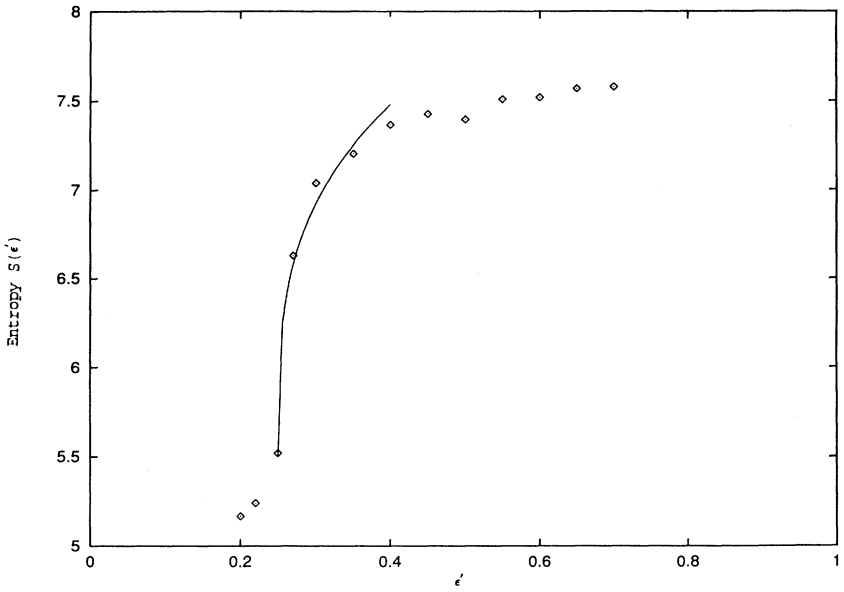

FIG. 6. The dependence of spectra entropy $S(\epsilon')$ for the pattern shown in Fig. 5 versus the control parameter ϵ'. Note that the curve increases rather rapidly near the value $\epsilon'_c = 0.25$, indicating the first appearance of defects which destroy the global parallel state. A fitting curve shows that $S(\epsilon') - S(\epsilon'_c) = A(\epsilon' - \epsilon'_c)^\alpha, \epsilon' > \epsilon'_c$, with $\alpha \approx 0.3$, $A \approx 3.5$, $S(\epsilon'_c) \approx 5.5$, and $\epsilon'_c = 0.25$.

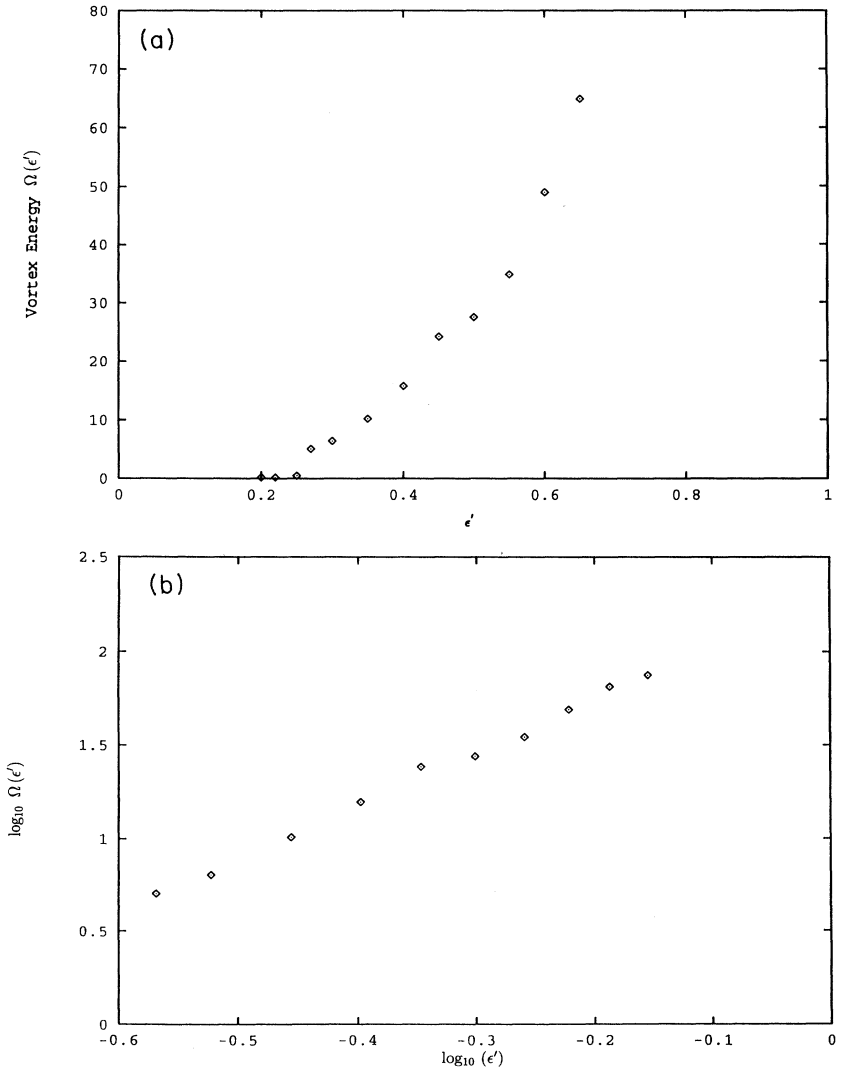

FIG. 7. (a) A plot showing the quantity $\Omega(\epsilon')$ as a function of the control parameter ϵ' for the same pattern sequence shown in Fig. 5. Again, note that there is a relatively sharp change in the curve at $\epsilon'_c = 0.25$. (b) A plot $\log_{10}(\Omega)$ vs $\log_{10}(\epsilon')$ showing that $\Omega(\epsilon') - \Omega(\epsilon'_c) = C(\epsilon' - \epsilon'_c)^\beta$, with $\Omega(\epsilon'_c) = 0.1$ and $\beta \approx 2.9$.

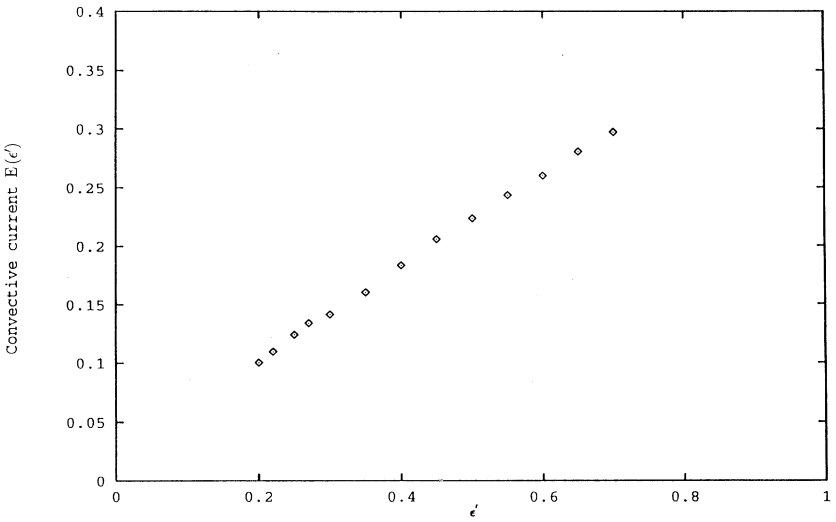

FIG. 8. The convective current $E(\epsilon')$ against the control parameter ϵ' for the same pattern sequence shown in Fig. 5. Note that there is no sign of a sudden change in the curve. The convective current increase linearly with the control parameter.

IV. TRANSITION TO SPATIOTEMPORAL SPIRAL CHAOS

An interesting question that has been discussed recently is whether or not the transition to spatiotemporal chaos is a phase transition somewhat similar to those encountered in critical phenomena. A number of quantities have been used to characterize such transitions, such as the defect density in the complex Ginzburg-Landau equation [27] and the distribution of laminar domain size in the Kuramoto-Sivashinsky model [28]. A more global approach has also been used to describe spatiotemporal chaos. There have been measurements of spatiotemporal chaos in Rayleigh-Bénard convection in annular cells [29]. In these experiments, an attempt has been made to characterize the transition to spatiotemporal chaos by introducing some global quantities, such as the spectra entropy and energy as a function of the control parameter.

In this section, we study the transition from the globally ordered parallel roll state to globally disordered but locally ordered spiral chaos state. One possible way to characterize this transition is to use the spectra entropy [30], which can be used to characterize either global order or spatiotemporal chaos. One of the advantages of using the spectra entropy is its relative ease of computation. It is computed from the power spectra, which may be calculated experimentally. The spectra entropy $S(\epsilon')$ is defined as

$$S(\epsilon') = -\left\langle \sum_{\vec{k}} (p_{\vec{k},t} \ln p_{\vec{k},t}) \right\rangle, \tag{6}$$

where $p_{\vec{k},t}$ is the relative weight of the spatial mode $\vec{k}$ in the power spectrum, and is defined as

$$p_{\vec{k},t} = \frac{|\psi^2(\vec{k},t)|}{\sum_{\vec{k}} |\psi^2(\vec{k},t)|} . \tag{7}$$

Here $\langle\,\rangle$ denotes a time average and ϵ' denotes a control parameter.

We choose the energy $E(\epsilon')$ to be the convective current, i.e.,

$$E(\epsilon') = \langle J(t) \rangle = \frac{1}{A} \left\langle \int \int \psi^2(x,y,t) dx dy \right\rangle. \tag{8}$$

Here A is the area of the domain.

We will also use another global measure which is related to the vertical vortex field (mean-flow field) during the transition to the spiral chaos state. As we discussed in the Introduction, for a global parallel roll state, the vortex field is identically zero everywhere. On the other hand, a localized spiral state has a nonzero vortex field. Furthermore, the transition from a global parallel roll state to a localized spiral chaos state indicates that there is broken symmetry. We define this quantity Ω as

$$\Omega(\epsilon') = \frac{1}{2A} \int \int \langle \omega_z^2(x,y,t) \rangle dx dy, \tag{9}$$

where

$$\omega_z = -\nabla^2 \zeta. \tag{10}$$

Ω is used as a means for measuring the amount of rotational activity inside the spiral structures. In fact, the density $\frac{1}{2}\omega_z^2$ is an important local quantity that measures directly the local spiral rotational velocity. It also serves as a measure of the order for the transition to the spatiotemporal chaos state. The quantity Ω is reminiscent of a Kolmogorov energy formulation in two-dimensional flow systems [31]. In the following, we present a numerical study of pattern formation of the convective roll state as a function of the control parameter (ϵ').

A. Spectra entropy $S(\epsilon')$

For each value of control parameter ϵ', we use a random initial condition (Gaussianly distributed with zero mean

and a variance 10^{-4}), with the same parameters as in Fig. 1. Figures 4(a)–4(j) show the different pattern configurations as a function of the control parameter. The existence of two different ordered regimes is clearly seen in Fig. 5: one is dominated by the global parallel roll state, and the other is dominated by the spatiotemporal spiral chaos state. The first appearance of defects which destroy the global parallel rolls and lead to the transition to the spiral chaos state occurs when the control parameter is $\epsilon' \approx 0.25$ [see Fig. 5(d)]. Figure 6 shows the dependence of the spectra entropy of the pattern structure versus the control parameter. The curve increases rather rapidly near the value $\epsilon'_c \approx 0.25$, indicating that there is a transition to the spiral chaos state. We have tried to quantitatively characterize the transition by computing S as a function of ϵ'. If one assumes that the transition can be described by a power behavior, i.e.,

$$S(\epsilon') - S(\epsilon'_c) = A(\epsilon' - \epsilon'_c)^{\alpha}, \quad \epsilon' > \epsilon'_c, \tag{11}$$

we find $\alpha \approx 0.3$, $A \approx 3.5$, $S(\epsilon'_c) \approx 5.5$, with $\epsilon'_c = 0.25$. Thus if this is a second-order transition, a rough estimate of the exponent α is about 0.3. We should also note that we would interpret $S(\epsilon'_c)$ as arising from boundary effects; i.e., we would expect $S(\epsilon'_c)$ to vanish for an infinite system. It is important to note, however, that our data are also consistent with a first-order phase transition, since due to the numerical limitations, and boundary effects, our resolution near the threshold is limited in the region $0.25 < \epsilon' < 0.27$.

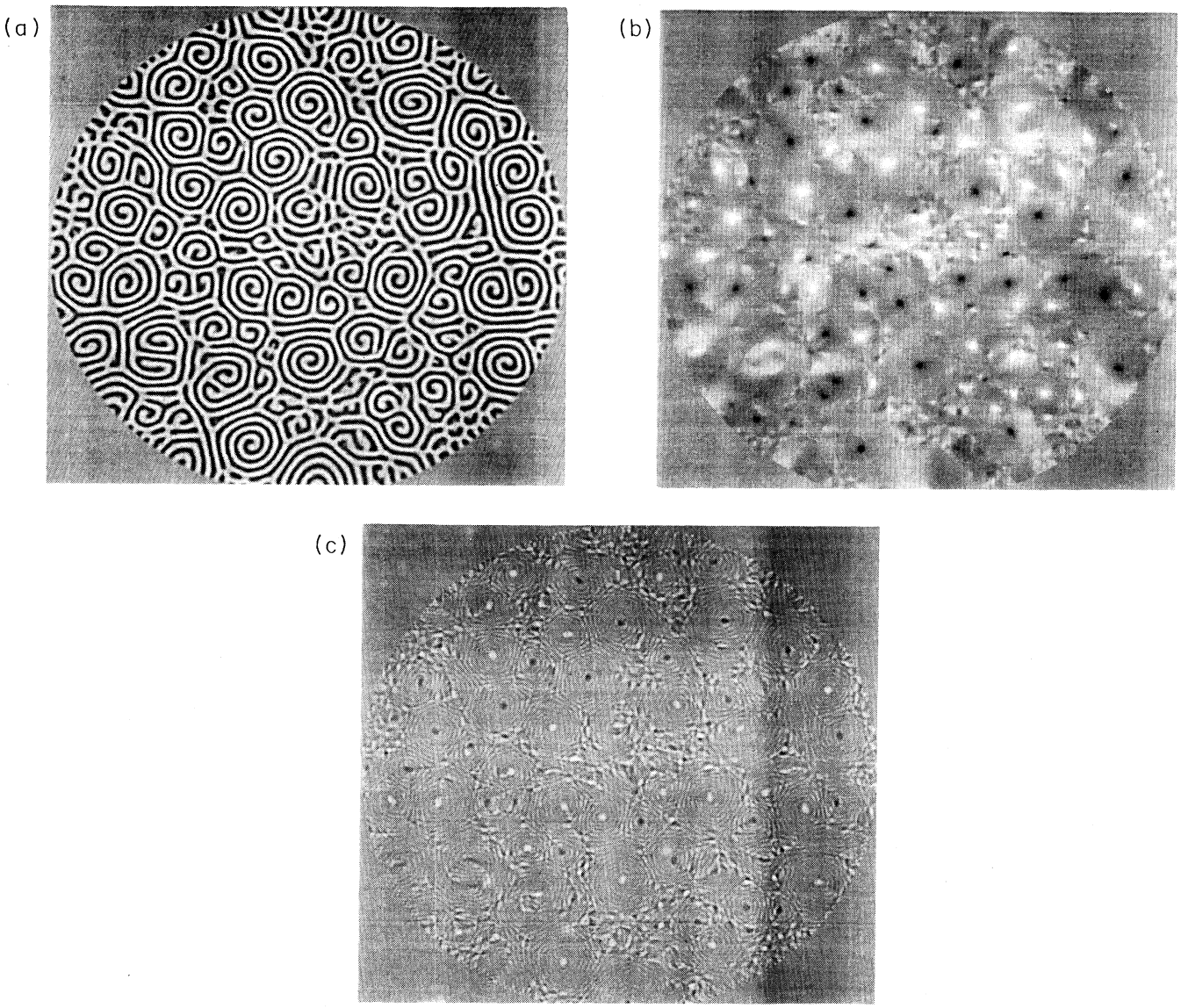

FIG. 9. (a)–(c) A snapshot of the spiral chaos state for a large aspect ratio of $\Gamma = 64$; (a) order parameter ψ, (b) mean flow ζ, and (c) vertical vorticity ω_z.

B. $\Omega(\epsilon')$

The transition to spiral chaos may also be characterized by measuring the quantity Ω, as a function of the control parameter. In Fig. 7(a), we plot Ω as a function of the control parameter ϵ'. Notice that there is a relatively sharp change in the curve at $\epsilon'_c \approx 0.25$ which marks a distinction between global parallel flow and spatiotemporal spiral flow. Again, the absence of a sharply defined critical point is possibly due to numerical limitations. We also observe that $\Omega(\epsilon')$ behaves according to a power law in the spiral chaos state: $\Omega(\epsilon') - \Omega(\epsilon'_c) = C(\epsilon' - \epsilon'_c)^\beta$, where $\Omega(\epsilon'_c) = 0.1$ and a rough estimate yields $\beta \approx 2.9 \pm 0.1$ as shown in Fig. 7(b). It would be interesting to verify our numerical results through experimental work.

C. Convective current $E(\epsilon')$

Figure 8 shows the numerical results of the time averaged convective current $\langle J \rangle$ versus the control parameter. One notices that the energy increases linearly with the control parameter, as one would expect for usual Rayleigh-Bénard convection at low Rayleigh number. There is no sign of a sudden change near the threshold $\epsilon'_c \approx 0.25$. This is in contrast to what happens in the "one-dimensional" Rayleigh-Bénard convection in the annular geometry [29], in which one observes a sharp increase near the transition to the spatiotemporal chaos state.

Finally, we have also studied spiral chaos in an even larger aspect ratio cell (Γ=64). Figure 9 shows a snapshot of the spiral chaos pattern formation obtained in the large cell. To study the effect of finite size on the spiral chaos state, we compared the spatial correlation functions $\langle C_\psi(r) \rangle$ obtained for a large aspect ratio $\Gamma = 64$ and an aspect ratio $\Gamma = 32$, respectively, and found that the two results are essentially identical.

V. CONCLUSION

We have presented numerical evidence for the existence of the spiral chaos state in the extended two-dimensional Rayleigh-Bénard convection system. Our numerical results are consistent with the observation of spatiotemporal spiral chaos in experiment. We have displayed the images of the large scale mean-flow field $\zeta(x, y, t)$ and the vertical vorticity $\omega_z(x, y, t)$ in a spiral chaos state. The vorticity field ω_z is very localized spatially and its dynamics is particlelike. These mean-flow and vorticity patterns have not been able to be studied in the experimental studies. Our simulations predict that there is a $1/f^2$ power-law behavior in the temporal dynamics of spiral defect chaos in a large aspect ratio system. A theoretical understanding of this $1/f^2$ noise is not yet known. The spiral chaos state is found to exist only for low Prandtl numbers and for large aspect ratios. These facts suggest that the large mean flow induces the spiral chaos state in a large aspect ratio system. We have characterized the spiral chaos state quantitatively through calculating the Fourier power spectra and spatial correlation functions, some of which (mean flow and vorticity) have not been measured in the experimental studies. We have also attempted to study the nature of the transition from the parallel roll to spiral chaos state, but have been unable to determine whether this is a sharp or gradual transition. Finally, we note that after our work was completed, we received unpublished results from Cross and Tu [32], who proposed a very interesting theory for spiral chaos. They argue that the dynamics of spiral defects is controlled by wave-number frustration instead of simply being driven by the mean-flow field. Further work on this subject is clearly necessary.

ACKNOWLEDGMENTS

We thank Jorge Viñals for many helpful discussions. This work was supported by the National Science Foundation under Grant No. DMR-9401985. The calculations reported here have been carried out on the Cray C-90 at the Pittsburgh Supercomputing Center.

[1] M. C. Cross and P. C. Hohenberg, Rev. Mod. Phys. **65**, 851 (1993).

[2] *Ordered and Turbulent Patterns in Taylor-Couette Flow*, Vol. 297 of *NATO Advanced Study Institute Series B: Physics*, edited by C. David Andereck and F. Hayot (Plenum, New York, 1992).

[3] J. P. Gollub and R. Ramshankar, in *New Perspectives in Turbulence*, edited by L. Sirovich (Springer-Verlag, New York, 1991), p. 165.

[4] P. Kolodner and C. M. Surko, Phys. Rev. Lett. **61**, 842 (1988); V. Steinberg and E. Kaplan, in *Spontaneous Formation of Space-Time Structures and Criticality*, Vol. 349 of *NATO Advanced Study Institute, Series C: Mathematical and Physical Science*, edited by T. Riste and D. Sherrington (Kluwer, Dordrecht, 1991).

[5] F. T. Arecchi, G. Giacomelli, P.L. Rammazza, and S. Risidori, Phys. Rev. Lett. **65**, 1579 (1990); J.V. Moloney and A. Newell, Physica D **44**, 1 (1990).

[6] P. Clavin, in *Physico Chemical Hydrodynamics*, edited by M. Velarde (Plenum, New York, 1988).

[7] G. Nicolis and I. Prigogine, *Self-Organization in Nonequilibrium Systems* (Wiley, New York, 1977); H. L. Swinney and V. I. Krinsky, Physica D **49**, 1 (1991); G. S. Skinner and H. Swinney, *ibid.* **48**, 1 (1991).

[8] G. Ahlers and R. P. Behringer, Prog. Theor. Phys. Suppl. **64**, 186 (1978); G. Ahlers, D. S. Cannell, and V. Steinberg, Phys. Rev. Lett. **54**, 1373 (1985); M. S. Heutmaker and J. P. Gollub, Phys. Rev. A **35**, 242 (1987); P. Manneville, *Dissipative Structures and Weak Turbulence* (Academic, New York, 1990).

[9] S. Morris, E. Bodenschatz, G. Ahlers, and D. S. Cannell, Phys. Rev. Lett. **71**, 2026 (1993).
[10] Y. Hu, R. E. Ecke, and G. Ahlers, Phys. Rev. Lett. **72**, 2191 (1994); **74**, 391 (1995); Phys. Rev. E **51**, 3263 (1995).
[11] M. Assenheimer and V. Steinberg, Nature **367**, 345 (1994).
[12] E. Bodenschatz, J. R. de Bruyn, G. Ahlers, and D. S. Cannell, Phys. Rev. Lett. **67**, 3078 (1991).
[13] M. Bestehorn, Phys. Lett. A **174**, 48 (1993).
[14] Haowen Xi, J. D. Gunton, and J. Viñals, Phys. Rev. Lett. **71**, 2030 (1993).
[15] Haowen Xi, J. Viñals, and J. D. Gunton, Phys. Rev. A **46**, R4483 (1992); Haowen Xi, J. D. Gunton, and J. Viñals, Phys. Rev. E **47**, R2987 (1993).
[16] M. Bestehorn, Phys. Rev. E **50**, 625 (1994).
[17] F. H. Busse, Rep. Prog. Phys. **41**, 1929 (1978).
[18] Y. Pomeau, Physica D **23**, 3 (1986).
[19] W. Decker, W. Pesch, and A. Weber, Phys. Rev. Lett. **73**, 648 (1994).
[20] J. Swift and P. C. Hohenberg, Phys. Rev. A **15**, 319 (1977).
[21] P. Manneville, J. Phys. **44**, 759 (1983).
[22] H. S. Greenside and W. M. Coughran, Jr., Phys. Rev. Lett. **49**, 726 (1982); Phys. Rev. A **30**, 398 (1984); H. S. Greenside and M. C. Cross, *ibid.* **31**, 2492 (1985).
[23] M. C. Cross, Phys. Fluids **23**, 1727 (1980); Phys. Rev. A **25**, 1065 (1982); **27**, 490 (1983).
[24] E. D. Siggia and A. Zippelius, Phys. Rev. Lett. **47**, 835 (1981); A. Zippelius and E. D. Siggia, Phys. Rev. A **26**, 1788 (1982); Phys. Fluids **26**, 2905 (1983).
[25] H. S. Greenside, M. C. Cross, and W. M. Coughran, Jr., Phys. Rev. Lett. **60**, 2269 (1988).
[26] We note that the horizontal diffusion time is Γ^2.
[27] B. I. Shraiman, A. Pumir, W. van Saarloos, P. C. Hohenberg, H. Chaté, and M. Holen, Physica D **57**, 241 (1992).
[28] H. Chaté and P. Manneville, Phys. Rev. Lett. **54**, 112 (1987); Physica D **32**, 409 (1988).
[29] M. Caponeri and S. Ciliberto, Physica D **58**, 365 (1992).
[30] G. C. Powell and I. C. Percival, J. Phys. A **12**, 2053 (1979).
[31] R. H. Kraichnan, Phys. Fluids **10**, 1417 (1967); G. K. Batchelor, *ibid.* Suppl. 2 **12**, 233 (1969).
[32] M. Cross and Yuhai Tu (unpublished).

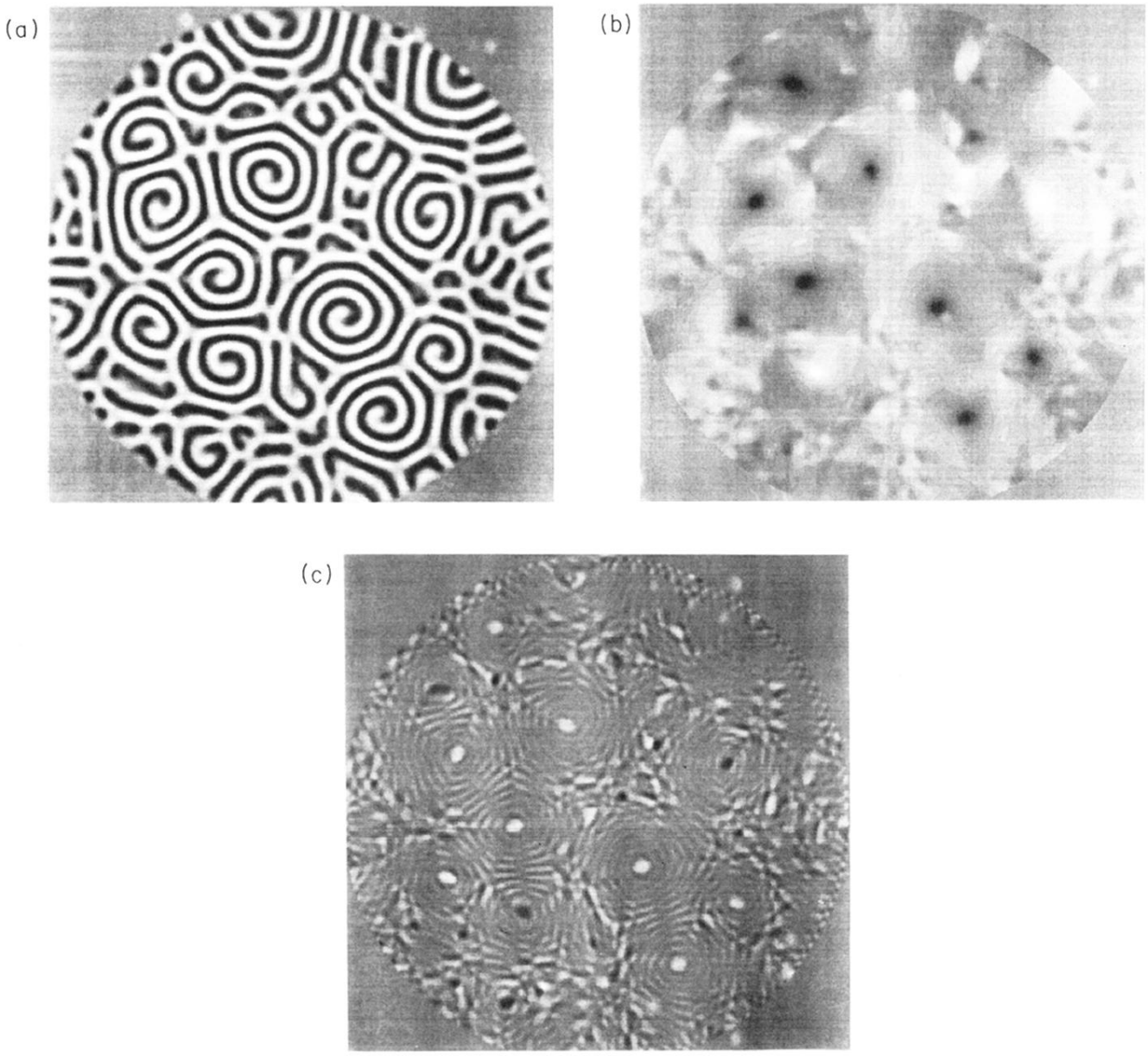

FIG. 1. (a) A typical configuration of the spiral chaos state. Dark regions correspond to hot rising fluid and white regions to cold descending fluid. The field $\psi(x, y, t)$ is shown here. Dark regions correspond to $\psi > 0$ and light regions to $\psi < 0$. (b) A snapshot of the mean-flow field $\zeta(x, y, t)$ that corresponds to the configuration shown in (a). White and dark regions correspond to clockwise and counterclockwise rotation of the spiral, respectively. (c) A snapshot of the vertical vorticity field $\omega_z(x, y, t)$ that corresponds to the configuration shown in (a). White and dark regions correspond to counterclockwise and clockwise rotation of the spiral, respectively. The configuration shown is $t = 900$.

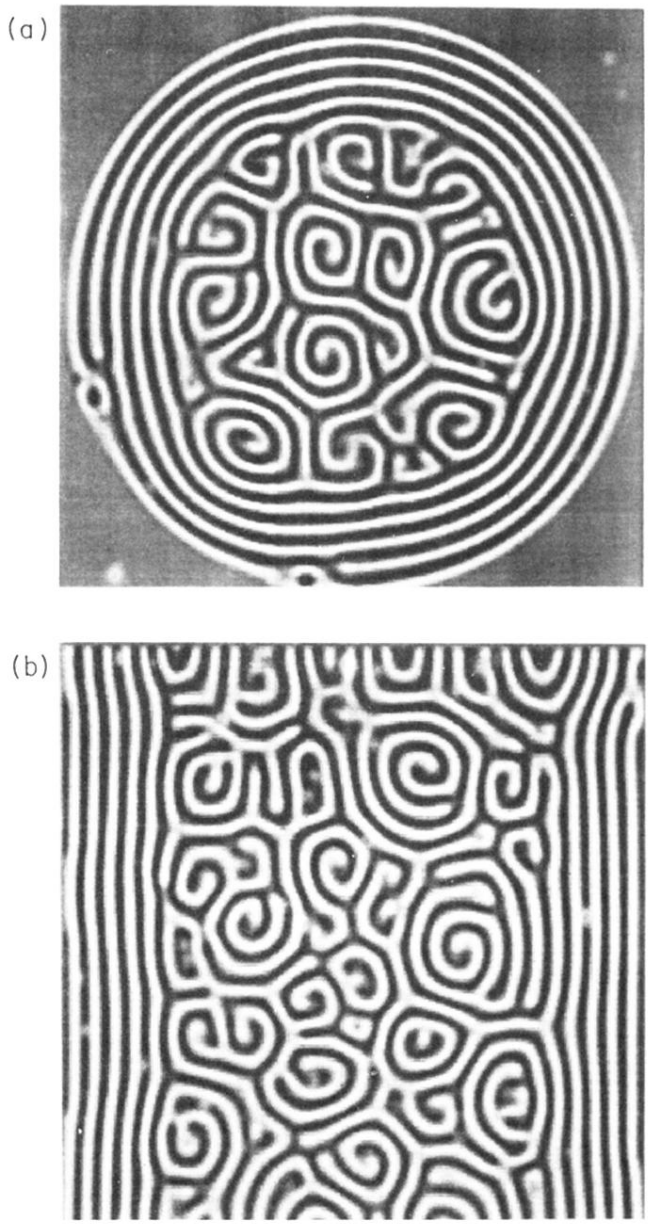

FIG. 4. Spiral chaos pattern formation in the presence of the sidewall forcing in (a) a cylindrical container and (b) a square container. The configuration shown has evolved from random initial conditions with aspect ratio $\Gamma = 32$. The values of the parameters used are $g_2 = 0$, $g_m = 50$, Pr=1, and $c^2 = 2$. The parameter ϵ' is quenched from 0 to 0.7, and a localized force field $f = 0.1$ near the wall was used in the simulation.

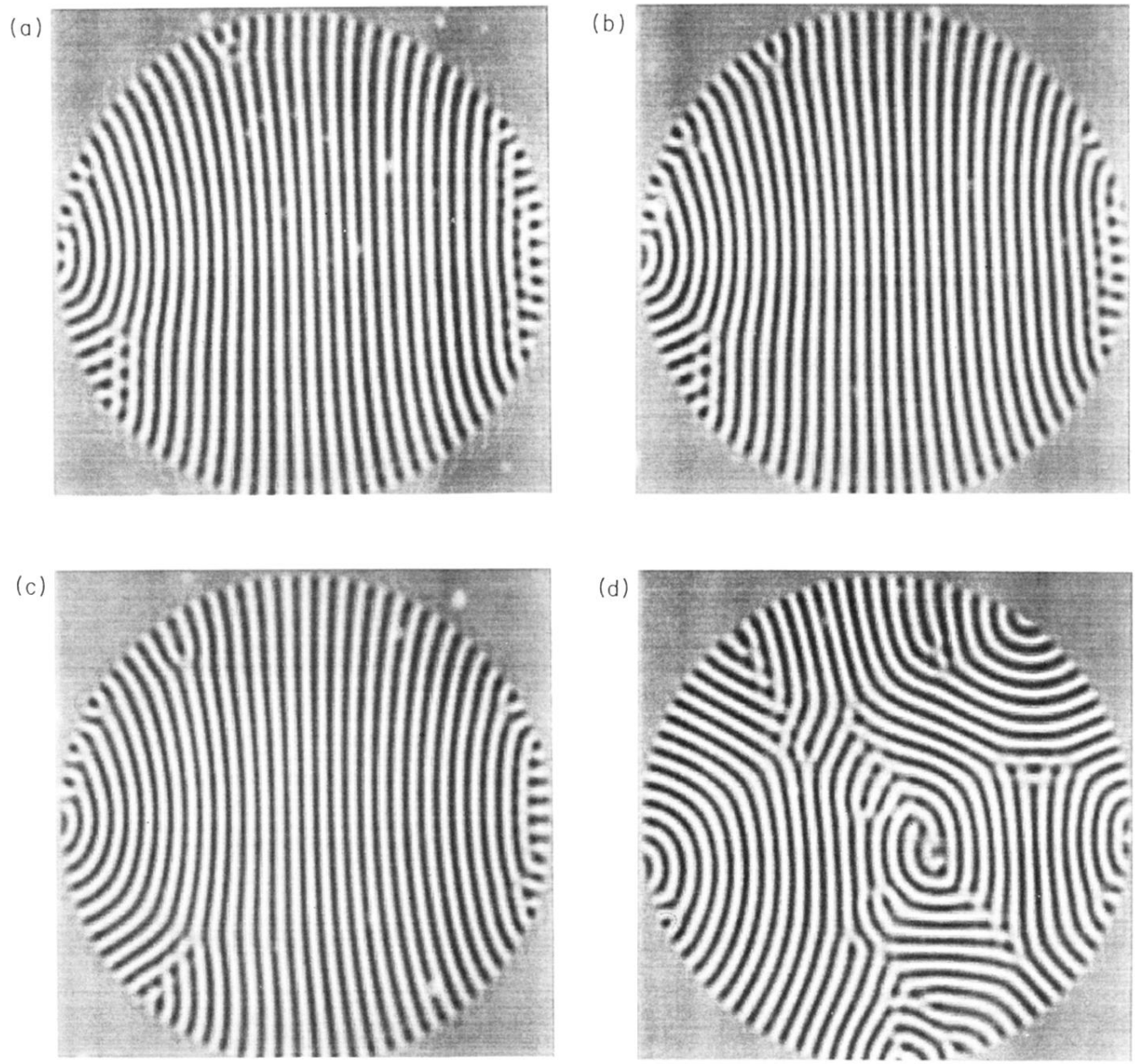

FIG. 5. (a)–(j) This sequence of configurations shows the typical convective pattern as a function of the control parameter ϵ'. One may distinguish between two different regimes: one is dominated by the global parallel roll state, the other is dominated by the spiral chaos state. The transition from global parallel roll to spiral chaos state occurs when $\epsilon'_c \approx 0.25$. The control parameters are (a) ϵ'=0.2, (b) ϵ'=0.22, (c) ϵ'= 0.25, (d) ϵ'= 0.27, (e) ϵ'= 0.3, (f) ϵ'= 0.35, (g) ϵ'= 0.4, (h) ϵ'= 0.5, (i) ϵ'= 0.6, and (j) ϵ'= 0.7. The values of the other parameters used are $g_2 = 0.35$, $g_m = 50$, $c^2 = 2$, and Pr=1.

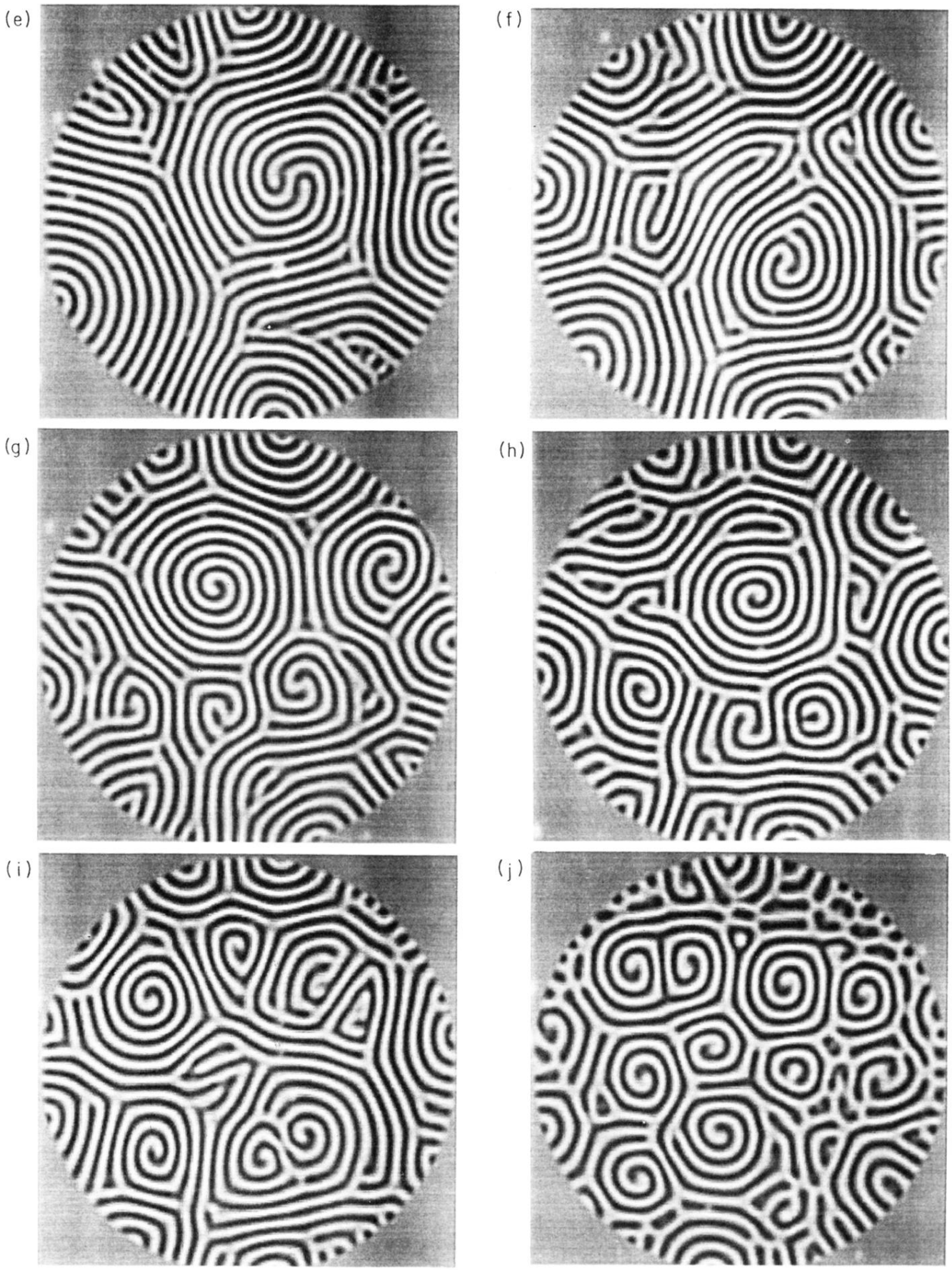

FIG. 5. (*Continued*).

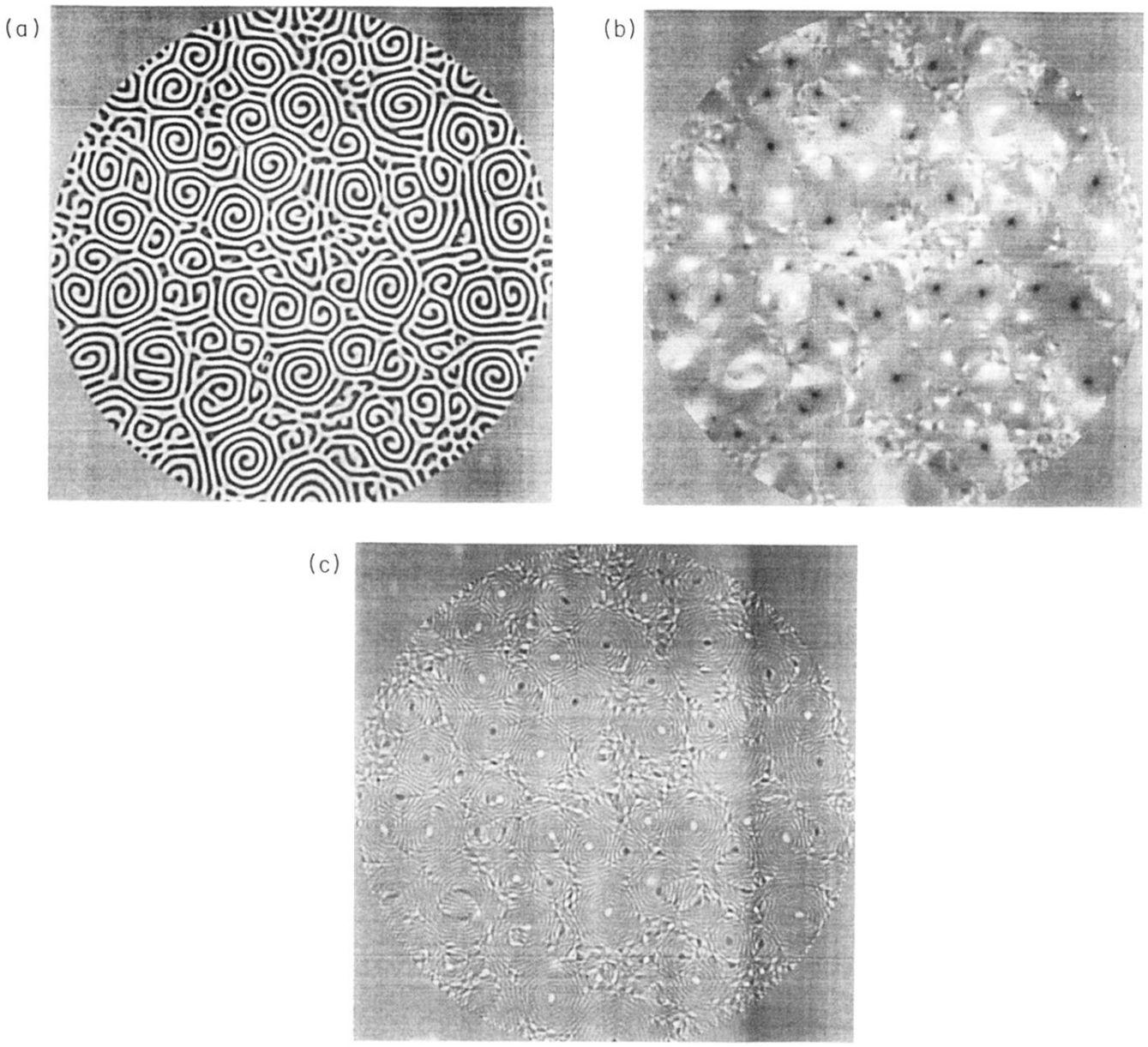

FIG. 9. (a)–(c) A snapshot of the spiral chaos state for a large aspect ratio of $\Gamma = 64$; (a) order parameter ψ, (b) mean flow ζ, and (c) vertical vorticity ω_z.